



Deposited via The University of Leeds.

White Rose Research Online URL for this paper:

<https://eprints.whiterose.ac.uk/id/eprint/81545/>

Article:

Dong, Z, Liu, S, Li, X et al. (2015) Influence of infiltration temperature on the microstructure and oxidation behavior of SiC-ZrC ceramic coating on C/C composites prepared by reactive melt infiltration. *Ceramics International*, 41 (1). pp. 797-811. ISSN: 1873-3956

<https://doi.org/10.1016/j.ceramint.2014.08.138>

Reuse

Items deposited in White Rose Research Online are protected by copyright, with all rights reserved unless indicated otherwise. They may be downloaded and/or printed for private study, or other acts as permitted by national copyright laws. The publisher or other rights holders may allow further reproduction and re-use of the full text version. This is indicated by the licence information on the White Rose Research Online record for the item.

Takedown

If you consider content in White Rose Research Online to be in breach of UK law, please notify us by emailing eprints@whiterose.ac.uk including the URL of the record and the reason for the withdrawal request.

Influence of infiltration temperature on the microstructure and oxidation behavior of SiC–ZrC ceramic coating on C/C composites prepared by reactive melt infiltration

Z.J. Dong^{a, b}, S. X. Liu^b, X.K. Li^{a, b, *}, A. Westwood^c, G.M. Yuan^b, Z.W. Cui^b, Y. Cong^b

^a The State Key Laboratory of Refractories and Metallurgy, Wuhan University of Science and Technology, Wuhan, Hubei 430081, PR China

^b The Hubei Province Key Laboratory of Coal Conversion & New Carbon Materials, Wuhan University of Science and Technology, Wuhan, Hubei 430081, PR China

^c Institute for Materials Research, University of Leeds, Leeds LS2 9JT, United Kingdom

Abstract

SiC–ZrC ceramic coating on C/C composites was prepared by reactive melt infiltration (RMI) using a powder mixture composed of Zr, Si and C as the infiltrator. The phase composition and microstructure of the ceramic coating were characterized by X–ray diffraction (XRD), scanning electron microscopy (SEM) and energy dispersive X-ray spectroscopy (EDS). The oxidation resistance of the as-prepared composites was tested at 1550 °C in static air. The results indicate that the infiltration temperature has remarkable effects on the phase composition and microstructure of the ceramic coating, as well as on the oxidation resistance of the composites. The SiC–ZrC coated C/C composites prepared at 2000 °C exhibit an excellent oxidation resistance. They gain weight about 5.9 wt% after oxidation at 1550 °C in static air for 5 h, whereas the SiC–ZrC coated C/C composites prepared at 1800 °C lose weight about 3.2 wt%. As a comparison, SiC coated C/C composites prepared at 2000 °C by

* Corresponding author. Tel/ Fax: +86 27 86556906.

E-mail address: xkli@21cn.com (X.K. Li)

RMI show an inferior oxidation resistance. After 5 h oxidation, SiC coated C/C composites are severely damaged and their weight loss reaches up to 44.3 wt%. The outstanding oxidation resistance of the SiC–ZrC coated C/C composites prepared at 2000 °C can be attributed to the rapid formation of a continuous glass-like layer composed of ZrO₂, ZrSiO₄ and SiO₂, which covers the surface of the composites and retards the oxygen diffusion and the attack on the underlying C/C substrate. For SiC coated C/C composites, the large SiC particles formed on the surface of the composites are difficult to oxidize rapidly and so a continuous and dense SiO₂ layer cannot be formed in time to significantly hinder fast oxygen diffusion leading to the consequent severe oxidation of the C/C substrate.

Keywords: Reactive melt infiltration; Weight loss; Glass-like layer; Oxidation resistance

1. Introduction

Carbon/carbon (C/C) composites have many unique properties, including low density, low coefficient of thermal expansion, high thermal conductivity, excellent high-temperature strength and good thermal shock resistance [1]. These outstanding properties make them as the leading structural materials used in high temperature environments such as rocket engines, nose tips, leading edges and other thermal protection systems for space vehicles [2]. Nevertheless, the rapid oxidation of C/C composites above 773 K limits their high temperature applications in oxygen containing environments [3]. Therefore, the key to extending applications of C/C composites is to develop reliable oxidation protection. It has been proved that introducing SiC ceramics into C/C matrix or forming a SiC coating on the C/C composites is very effective for improving the oxidation resistance of C/C composites at high temperatures [4-7]. The improved oxidation resistance of SiC coated C/C composites can

be mainly attributed to the formation of silica glass with self-healing capability and low oxygen permeability during the oxidation of SiC at high temperatures, and this glass can act as a diffusion barrier to prevent oxygen from diffusing into the C/C matrix. However, due to the active oxidation of SiC and gradual volatilization of silica glass above 1600 °C, the maximum working temperature of SiC coated C/C composites is also limited to about 1600 °C [8, 9]. For that reason, refractory metal carbides/borides (e.g. ZrC, HfC, TaC, ZrB₂, etc.), known as ultra high temperature ceramics (UHTCs), has been introduced into SiC coated C/C composites. The UHTCs modified SiC coated C/C composites have retained strength and good ablation resistance at temperatures over 1600 °C, which allow them to be used as the potential candidates for extreme environments associated with the hypersonic flight and rocket propulsion [10, 11]. Among those UHTCs, ZrC has been given much attention because of its high melting point (3540 °C), relatively low density (6.73 g/cm³), high thermal conductivity, excellent chemical stability and thermal shock resistance [12, 13]. In addition, the zirconia (ZrO₂) formed by the oxidation of ZrC has a melting point as high as 2700 °C. It could form a protective layer on the surface of C/C matrix at ultra high temperatures so as to effectively reduce the diffusion of oxygen, which will result in the significant improvement in the ablation resistance of C/C composites. Therefore, in the last few years, many efforts have been made to obtain composites with improved oxidation and ablation resistance by introducing ZrC–SiC ceramics into C/C matrix. The methods of incorporation of ZrC–SiC ceramics into C/C matrix include slurry impregnation [8,14], chemical vapor deposition (CVD) [15], polymer impregnation, pyrolysis (PIP) [16-19] and reactive melt infiltration (RMI) [11,13, 20-23]. Compared with other methods, RMI is rapid, simple and cheap and can be used to fabricate components with complex geometries [24, 25]. During the process of

RMI, the ZrC–SiC ceramics are formed both inside and outside of the composites by the reaction between the porous C/C matrix and the infiltrated metal melt. The driving force for infiltration is capillarity and this process lasts from minutes to hours. Recently, SiC–ZrC ceramic coating on C/C composites has been successfully fabricated by RMI, in which the infiltration powder was $\text{Si}_{0.87}\text{Zr}_{0.13}$ alloy [11] or mixed powders of Zr, ZrO_2 , Si and C [13, 20-23]. However, most of these reports are focused on the investigation of the mechanical and ablation properties of the SiC–ZrC coated C/C composites. The effects of RMI parameters on the microstructure of the ceramic coating and oxidation resistance of the composites are rarely reported.

In this work, SiC–ZrC ceramic coating on C/C composites was prepared by RMI using a powder mixture composed of Zr, Si and C as the infiltrator. The influence of infiltration temperature on the phase composition and microstructure of the ceramic coating was investigated in detail. The oxidation resistance of the SiC–ZrC coated C/C composites was tested in static air at 1550 °C and was further related to their microstructure in order to clarify the oxidation resistance mechanism.

2. Experimental details

Small cubic specimens (10×10×10 mm) to be used as substrates were cut from a 3D C/C composite bulk with a density of about 1.60 g/cm³. Before the process of RMI, each specimen was hand-polished with 400 grit SiC paper, then cleaned ultrasonically with ethanol and dried at 100 °C for 1 h. The powder mixture used as the infiltrator was composed of Si (300 mesh), Zr (300 mesh) and C (300 mesh) with a mass ratio Si: Zr: C of 1: 1: 0.3. All of the above powders were of analytical grade and commercially available. The Si, Zr and C powders were

blended in a ball mill for 20 h. The cubic C/C specimens, embedded in the powder mixture, were placed in a graphite crucible with a graphite lid, and then heat-treated at 1800 °C, 1900 °C, and 2000 °C for 2 h in an induction furnace under a flowing argon atmosphere, followed by natural cooling down to room temperature. The C/C composites with a SiC–ZrC ceramic coating were then retrieved from the mixture, and ultrasonically cleaned to remove any loosely embedded powders. The SiC–ZrC coated C/C composites thus prepared at 1800 °C, 1900 °C, and 2000 °C were labeled as SZ18, SZ19 and SZ20, respectively. For comparison, the SiC coated C/C composites labeled as S20 were prepared at 2000 °C by the same method using a powder mixture of Si and C with a mass ratio Si: C of 2: 0.3 as the infiltrator.

The isothermal oxidation tests for the as-prepared SiC–ZrC coated C/C and SiC coated C/C composites were carried out in an alumina tube furnace. Before the isothermal oxidation test, all of the samples were dried at 120 °C to constant weight. After the furnace had been heated up to 1550 °C, the samples were directly pushed into the furnace and exposed to static air for a given period of time and then pulled out and cooled to room temperature in air for weighing. The weight of the samples after oxidation was measured with an analytical balance with a sensitivity of ± 0.1 mg (Mettler Toledo, AL 104, Switzerland) and then the oxidized samples were put into the furnace again for the next oxidation period. Cumulative weight changes of the samples were calculated and reported as a function of the oxidation time.

The phase composition of the as-prepared samples before and after oxidation was identified by an X-ray diffraction (XRD) instrument (Philips X'Pert Pro MPD) using Cu-K α radiation ($\lambda=1.54056$ Å). The working voltage and current of the Cu target were 40 kV and 40 mA, respectively. A field emission gun scanning electron microscope (FESEM, NOVA400

NANOSEM) was used to examine the surface morphology of the samples before and after oxidation. The elemental composition and distribution within the surface and the interior of the samples were determined by energy dispersive X-ray spectroscopy (EDS, attachment to the SEM).

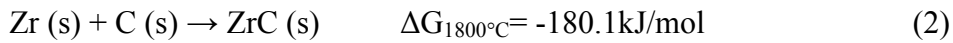
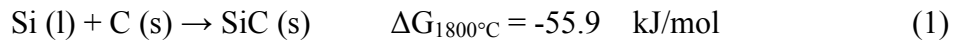
3. Results and Discussion

3.1 Preparation of the SiC–ZrC ceramic coating on C/C composites

Fig. 1 shows the morphology and void distribution of the porous C/C composites with a density of 1.60 g/cm^3 that was prepared by chemical vapor infiltration (CVI). As can be seen from Fig. 1a and b, there are two kinds of pores in the C/C composites. Small pores are located inside fiber bundles, while large pores exist among the carbon fiber bundles and fiber layers. The large inter-bundle and inter-layer pores are difficult to fill completely by pyrolytic carbon (PyC) deposition in a short time and are considered to be the infiltration channels for the melted powders during the RMI process. Fig. 1c shows the microstructure of a fiber bundle inside the C/C composites. It can be seen that a PyC coating with a thickness of about $1\text{-}2 \text{ }\mu\text{m}$ is uniformly deposited on the surface of the carbon fiber filaments and there are still some micro-pores that are not fully filled by PyC in the carbon fiber bundle. Some individual PyC-coated carbon fibers in large pores are shown in Fig. 1d. It is very interesting to note that the PyC coating formed on these carbon fibers has a multi-layer structure. The thickness of the PyC coating is about $5 \text{ }\mu\text{m}$, much higher than that of the PyC coating formed on the carbon fibers in the fiber bundle shown in Fig. 1c. The PyC coating deposited on the carbon fibers is believed to be helpful for improvement of the stiffness of carbon fiber preform and for preventing damage to the carbon fibers in the subsequent RMI processing.

Fig. 2 shows the XRD patterns of the surface and the cross section of samples prepared at different infiltration temperatures. For sample SZ18 prepared at a relatively low infiltration temperature, only SiC and a few very weak ZrC diffraction peaks can be observed from the surface XRD pattern, as shown in Fig. 2a. No detectable ZrC diffraction peaks appear in the cross section XRD pattern (Fig. 2b), which indicates that ZrC is not formed inside the C/C composite at a relatively low infiltration temperature. As the infiltration temperature increases to 1900 °C, the relative intensity of the ZrC diffraction peaks increases, while the relative intensity of the SiC diffraction peaks decreases, as can be seen from the surface XRD pattern of sample SZ19 (Fig. 2a). In addition, a small amount of ZrSi₂ phase is detected on the surface of sample SZ19, but it is not found inside it (Fig. 2b). This phenomenon can be explained from the fact that the ZrSi₂ infiltrated into the C/C substrate is depleted by reacting with carbon to form ZrC and SiC ceramics during the RMI process, whereas at the surface, unreacted carbon is not available in sufficient quantities for this to occur completely. Further increasing the infiltration temperature to 2000 °C, the surface and the cross section phase compositions of sample SZ20 remain practically unchanged excepting the appearance of residual Zr phase on the surface as compared with those of sample SZ19. However, for sample S20, the surface XRD pattern shows only SiC diffraction peaks, and no residual Si diffraction peaks can be observed (Fig. 2a). It should also be noted that no distinct carbon diffraction peaks appear in the surface XRD patterns of any of the samples, which means that the surfaces of the composites are completely covered by single-phase SiC or multiphase SiC-ZrC-ZrSi₂ layer. In contrast, the cross section XRD patterns of all of the samples show obvious broad carbon peaks arising from the carbon fibers and the residual pyrolytic carbon (Fig. 2b).

It is believed that the formation of the SiC and ZrC phases on the surface of the composites is due to the reaction of carbon with silicon and zirconium, respectively. The relevant reactions and thermodynamic parameters are as follows:



The formation of ZrC is expected to be more favorable than that of SiC due to the much more negative Gibbs free energy for ZrC, but this is inconsistent with the experimental results. This suggests that the formation reactions of ZrC and SiC are more likely to be under kinetic rather than thermodynamic control. As a matter of fact, Zr powder has a melting point of 1850 °C [26], which is much higher than that of the Si powder (1410 °C) and so, when the melt infiltration temperature is 1800 °C, the Si is molten and diffuses rapidly to the surface of the C/C substrate, then reacting with carbon to form SiC ceramic. However, the Zr is still solid and has a higher relative atomic weight, and as a result, the diffusion rate of Zr is much lower than that of the molten Si, which leads to a much lower growth rate of ZrC. As the melt infiltration temperature rises above the melting point of Zr, some of the liquid Zr will react with Si to form ZrSi₂, while the rest will react with carbon to form ZrC ceramic, and the reaction rate increases rapidly due to the liquid phase diffusion now becoming possible in the system.

3.2 Structure of the SiC–ZrC ceramic coating on C/C composites

Fig. 3 shows the low magnification SEM images of the surface and the cross section of the samples prepared at various infiltration temperatures. As can be seen from Fig. 3a, when the melt infiltration temperature is 1800 °C, a thin ceramic coating composed of SiC and ZrC is formed on the surface of sample SZ18, and the outline of the fiber bundle can be observed

clearly. Fig. 3b shows the morphology of the cross section of sample SZ18. It can be seen that large pores are still present in the C/C substrate, indicating that only a small amount of ceramic has been formed in the composite after the RMI process. When the melt infiltration temperature increased to 1900 °C, the thickness of the ceramic coating, on sample SZ19, increases markedly, and as a result, the profile of the fiber bundle can no longer be seen any more, although some large holes are still found on the surface of the composites because of incomplete filling (Fig.3c). Compared with sample SZ18, sample SZ19 shows a relatively low porosity and a dense internal structure, as shown in Fig. 3d. The relatively low porosity is largely due to the fact that extensive ZrC and SiC ceramic formation during the RMI process at 1900 °C effectively fills both the large pores among the fibre bundles and some small apertures inside the fiber bundles. It is well known that, at a higher temperature, the fluidity of molten metal will increase since the viscosity decreases [27]. Thus, increasing the infiltration temperature facilitates the infiltration process and at the same time accelerates the reaction between the melt and carbon. Upon further increasing the infiltration temperature to 2000 °C, the number of the large pores on the surface of sample SZ20 appears to decrease, accompanied by the occurrence of some micro-cracks (Fig. 3e). From Fig. 3f, it can be seen that the cross section morphology of sample SZ20 is similar to that of sample SZ19. Some crevices observed inside sample SZ20 may be generated from the process of sample cutting and polishing for SEM observation. Fig. 3g and h show the structure of the surface and cross-section, respectively, of sample S20. The surface of sample S20 consists of coarse crystalline SiC particles and there are some large cracks that are probably caused by the differential thermal expansion coefficient between the coating and matrix during cooling after high temperature infiltration. There is no distinct difference between the cross sectional

morphologies of samples SZ20 and S20.

Fig. 4 shows typical higher magnification SEM images of the surface and cross section of the ceramic coatings on the product samples. It can be seen clearly from Fig. 4a that the ceramic coating on sample SZ18 has a rough surface and mainly consists of nano-sized grains (top inset in Fig. 4a). The ceramic coating is too thin for its thickness to be estimated using the SEM scale bar in Fig. 4b. The nano-sized coating grains and a very low coating thickness indicate that infiltration of Si and Zr metals at 1800 °C is not conducive to the formation and growth of SiC-ZrC ceramics either outside or inside the C/C substrate. The surface morphology of the ceramic coating on sample SZ19 is shown in Fig. 4c. It reveals that three kinds of crystalline particles characterized as dark grey, light grey and white are formed on the coating surface. EDS analysis shown in Fig. 5a reveals the dark grey phase is composed of Si and Zr. Based on a combination of the XRD results (Fig. 2a) with EDS analysis, it can be identified as $ZrSi_2$ derived from the reaction between Si and Zr. The light grey phase shown in Fig. 4c has a polyhedral structure, is composed of Si and C (Fig. 5b) and can be assigned as SiC. The white phase shown in Fig. 4c mainly consists of Zr and C, and can be identified as ZrC (Fig. 5c). The weak Si peak in the EDS pattern is possibly caused by the interference of SiC around the detection point. Fig. 4d shows the cross sectional morphology of the ceramic coating on sample SZ19. The ceramic coating has a dense structure without penetrating cracks or large holes and the average thickness is estimated to about 80 μm . Furthermore, the ceramic coating is integrated well with the underlying C/C substrate, which is beneficial for the improvement of the thermal shock resistance of the coating. Fig. 4e displays the surface morphology of the ceramic coating on sample SZ20. It reveals that the coating surface consists of grey and white phases. According to the EDS (Fig. 5d-f) and XRD (Fig. 2a)

analysis, the white phase, the grey phase with a polyhedral structure and the grey phase with a worm-like structure can be assigned as ZrC, SiC and a mixture of Zr and ZrSi₂, respectively. The average thickness of the coating on sample SZ20 is estimated to be about 110 μm, obviously larger than that of the coating on sample SZ19 (Fig. 4f), and there is no obvious interface between the coating and the underlying C/C substrate. A careful comparison of Fig. 4c with Fig. 4e reveals that the mean size of SiC particles significantly increases as infiltration temperature increases from 1900 °C to 2000 °C. Fig. 6 shows a linear EDS analysis in a cross section of the ceramic coating on sample SZ20. It can be seen that the concentrations of Si, Zr and C fluctuate greatly across the coating as a result of the inhomogeneous distribution of the pores in the C/C substrate. The abundance of Si is generally much higher than that of Zr taking the cross section as a whole, which is in agreement with the result of XRD analysis shown in Fig. 2b. In addition to this, Zr and Si are also present inside the C/C substrate, suggesting that the molten Zr and Si have good fluidity at 2000 °C and can be easily infiltrated into the substrate. The above observation of the morphologies of the ceramic coatings on samples SZ18, SZ19 and SZ20 also indicates that the thickness and compactness of the coating increase with increasing infiltration temperature. The C/C composites with a dense coating are expected to exhibit better oxidation resistance. As a comparison, the surface and cross sectional morphologies of the single-phase SiC coating formed on sample S20 are displayed in Fig. 4g and h, respectively. As can be seen from Fig. 4e and g, the grains of the SiC coating have a wide size distribution from a few micrometers to tens of micrometers, and the average grain size of the SiC formed on sample S20 is much larger than that of the SiC formed on sample SZ20. In addition, the single-phase SiC coating shows a relatively loose structure and many voids can be observed in the coating. These voids may increase the inner

surface of the composites and provide channels for oxygen diffusion, which also become active points during oxidation for the adsorption of and reaction with oxygen. Therefore, it might be anticipated that the oxidation resistance of sample S20 is inferior to that of sample SZ20, even though the thickness of the single-phase SiC coating formed on sample S20 is about 200 μm , i.e. much larger than that of the multiphase coating formed on sample SZ20.

In order to gain more detailed insight into the microstructure of the inner fibers in the obtained composite products, images of individual carbon fibers inside large voids were obtained and are presented in Fig. 7. The large voids are located close to the interface between the ceramic coating and C/C substrate. It can be seen that the surfaces of the individual carbon fibers are all covered by a coating. The coating grains not just physically adhere to the fiber surfaces but truly chemically bond to the fiber surfaces through the in situ carbothermal reaction between Si, Zr and the PyC deposited on the carbon fibers. When the infiltration temperature is 1800 $^{\circ}\text{C}$, the grain size and the thickness of the coating formed on the carbon fibers are relatively small, as shown in Fig. 7a. Thus, the coating cannot provide sustainable protection for the carbon fiber during the oxidation of sample SZ18. When the infiltration temperature increases to 1900 $^{\circ}\text{C}$, the grain size and the thickness of the coating increase markedly (Fig. 7b). In addition, it is interesting to note that there are some flaky particles with a size of about 10 μm adhering to the coating surface. As the infiltration temperature increases to 2000 $^{\circ}\text{C}$, there is no distinct changes in the grain size and the thickness of the coating on the fibers (Fig. 7c). The dense ceramic coatings formed on the surfaces of the individual carbon fibers inside samples SZ19 and SZ20 are expected to protect the carbon fibers from oxidation for extended periods. Fig. 7d shows the surface morphology of the individual carbon fibers inside sample S20. The average size of the grains formed on the carbon fibers

inside sample S20 is much larger than that of the grains formed on the carbon fibers inside samples SZ19 and SZ20. As a result, the fibers inside the sample S20 are not covered completely by the SiC coating. A large number of pores exist among the grains, through which oxygen will diffuse quickly onto the fiber surface and thereby cause the erosion of the fiber under oxidizing conditions.

3.3 Oxidation properties of the SiC–ZrC coated C/C composites

In order to investigate the effect of the infiltration temperature on the oxidation resistance of the obtained SiC–ZrC coated C/C and SiC coated C/C composites, the isothermal oxidation tests on samples SZ18, SZ19, SZ20 and S20 were carried out in static air at 1550 °C. Fig. 8 shows the weight changes of these composites as a function of oxidation time. As expected, samples SZ18, SZ19 and SZ20 exhibit much better oxidation resistance than that of sample S20. The weight loss of the sample S20 increases almost linearly with oxidation time throughout the oxidation process. After oxidation for 1 h, the weight loss of the sample S20 is about 5.6 wt%. As the oxidation time increases to 5 h, its weight loss increases up to 44.3 wt%. As is well known, the oxidation of carbon will lead to the weight loss from the sample, while oxidation of ZrC, ZrSi₂ and SiC will result in sample weight gain. Therefore, the continuous weight loss of sample S20 implies the intense oxidation of the C/C substrate from the beginning. In contrast to sample S20, samples SZ18, SZ19 and SZ20 experience a weight gain of about 2.7 wt% after 1 h of oxidation. This suggests that any weight gain from the oxidation of SiC, ZrC and ZrSi₂ outweighs any weight loss from the carbon oxidation. With increasing duration of oxidation, the weight gains of both samples SZ19 and SZ20 increase steadily. After 5 h of oxidation, samples SZ19 and SZ20 gain weight about 4.1 wt% and 5.9 wt%, respectively. However, the weight of sample SZ18 decreases

gradually after the initial 1 h of oxidation and its weight loss increases to 3.2 wt% after 5 h of oxidation, thus displaying an inferior oxidation resistance as compared with that of sample SZ19 and SZ20. These isothermal oxidation tests suggest that the infiltration temperature has a remarkable influence on the oxidation resistance of the obtained composite products; i.e. increasing the infiltration temperature improves the oxidation resistance of the obtained SiC–ZrC coated C/C composites.

Fig. 9 shows the surface and the cross sectional morphologies of the oxidized samples. It can be seen from Fig. 9a that the surface of the oxidized sample SZ18 is covered by a discontinuous glass-like coating. Since the coating formed on the surface of the sample is very thin, many large pores are not sealed and still exist inside the fiber bundles with an orientation normal to the surface. The XRD analysis shown in Fig. 10a reveals that the glass-like layer mainly consists of SiO₂, ZrSiO₄ and SiC. The ZrO₂ phase is derived from the oxidation of ZrC, while the ZrSiO₄ phase which is believed to possess an excellent high temperature oxidation resistance [28], results from the reaction between ZrO₂ and SiO₂ itself formed by the oxidation of SiC. After oxidation at 1550 °C for 5 h in static air, the number and the size of the pores inside sample SZ18 increase remarkably (Figs. 3b and 9b), as a result of the oxidation of part of the PyC-coated carbon fibers in the C/C substrate. This indicates that the thin and discontinuous glass-like layer formed on the surface of sample SZ18 can only provide limited oxidation protection for the C/C substrate. The oxidized sample SZ19 exhibits a surface morphology quite different from that of the oxidized sample SZ18. After 5 h of oxidation, a large quantity of SiC, ZrC and ZrSi₂ grains on the surface of the sample SZ19 are oxidized and coalesced to form a continuous and rugged glass-like layer that seals the cracks and pores on the surface of the C/C substrate (Fig. 9c). The phase composition of the

glass-like layer, as shown in Fig.10a, includes ZrSiO_4 , SiO_2 , ZrO_2 and SiC . It has been reported that the continuous SiO_2 glassy layer possesses very low oxygen permeability and that ZrSiO_4 derived from it can further improve its stability and lower the diffusion rate of oxygen in the oxide layer, thereby endowing it with the excellent oxidation resistance at high temperature [28, 29]. Owing to the effective protection provided by the glass-like coating, the inner morphology and structure of the C/C substrate are almost intact (Figs. 3d and 9d) and no oxide phases are detected inside sample SZ19 after 5 h of oxidation as shown in Fig. 10b. Moreover, the glass-like layer is integrated well with the C/C substrate. No debonding or large cracks are observed, suggesting a high bonding strength and good thermal expansivity compatibility between them. Fig. 9e shows the surface morphology of the oxidized sample SZ20. It can be seen that the surface of the oxidized sample is covered by a smooth glass-like layer with many melt bubbles, which are assumed to be formed during the escaping of the gases (SiO , CO or CO_2) produced by oxidation of the ceramic coating. XRD analysis confirms that the melt layer has the same phase composition as that covering on sample SZ19. The intensities of the diffraction peaks of SiO_2 , ZrSiO_4 and ZrO_2 formed on sample SZ20 are much stronger than those formed on sample SZ19, indicating a thicker glassy oxide layer covering on sample SZ20 after oxidation for 5 h. Additionally, due to the mismatch of the thermal expansion coefficient (CTE) between the C/C substrate and the glass-like layer, a few micro-cracks are generated on the coating surface during rapid cooling of the sample. In view of the fact that the oxide glass has good fluidity at high temperature, these micro-cracks are expected to self-heal when sample SZ20 is heated to 1550 °C again. Fig. 11 shows the variation of C, Si, Zr and O content from the surface to the interior of the glass-like layer. Unlike the elemental C, Si and Zr, the O exhibits a gradient distribution. The O content close

to the coating surface is apparently higher than that in the interior of the coating. This further confirms that the glass-like layer can act as a diffusion barrier to block inward transfer of oxygen during the oxidation test. With effective protection by the glass-like oxide layer, the internal C/C substrate shows no significant change in its morphology and structure after 5 h of oxidation (Figs. 3f and 9f) and no diffraction peaks from SiO₂ and ZrO₂ are observed in the XRD pattern of the cross section of the oxidized sample SZ20 (Fig. 10b). However, for sample S20, after 5 h of oxidation, the small SiC particles on its surface are highly oxidized and coalesced to form a discontinuous glass-like layer with many cavities distributed in some discrete local regions of the coating (Fig. 9g). In contrast, the large SiC particles are only slightly oxidized, as confirmed by EDS analysis (not shown). As reported in the literature [30, 31], the oxidation rate of the carbide particles strongly depends on the particle size. Small carbide particles possess a large surface area and can be rapidly oxidized in a short time to form a continuous and uniform glass film covering the surface of the composites. On the other hand, the large carbide particles have relatively lower surface area and it takes a longer time for a continuous and uniform glass film to form. Therefore, where a significant proportion of SiC is in the form of large particles, as in sample S20, before a continuous and uniform SiO₂ glass film is formed, the cavities and voids in the coating are possible channels accessible to transport oxygen into the interior of the composite, thus accelerating the oxidation of the C/C substrate. As can be seen from Fig. 9h, after 5 h of oxidation, the C/C substrate has been severely damaged and some large holes are evident inside the oxidized sample S20, which are assumed to be generated by the oxidation of the carbon fiber bundles. In addition, weak diffraction peaks of SiO₂ are also observed in the XRD pattern of the cross section of the oxidized sample S20 (Fig. 10b). This suggests that single-phase SiC coating cannot protect

C/C composites from oxidation effectively. The above SEM observations for the oxidized samples agree well with the results of the isothermal oxidation tests presented in Fig. 8.

Fig. 12 shows representative morphologies of individual fibers and fiber bundles close to the surface of the oxidized samples. A careful comparison of Fig. 12a with Fig. 7a reveals that the coating grains formed on the individual fibers inside sample SZ18 during the RMI process are oxidized and coalesced to a glass-like layer after 5 h of oxidation. Because the resulting glass-like coating is very thin and has many pinholes, oxygen can diffuse easily from the surrounding atmosphere into the PyC coating and react with the carbon, finally leading to the degradation of the carbon fiber. The morphology of the fiber bundles inside the oxidized sample SZ18 is shown in Fig. 12b. It can be seen clearly that the diameter of a large amount of carbon fiber filaments reduces significantly due to oxidation and as a result an annular gap becomes visible between the carbon fiber core and the PyC coating. This implies that the carbon fiber filaments are more prone to oxidation than the PyC coating. However, the individual carbon fibers inside both the oxidized samples SZ19 and SZ20 (Fig. 12c and e) seem to be immune from attack by oxygen in air due to the effective protection by the continuous and dense coatings that are mainly composed of ZrC and SiC. Furthermore, it is interesting to note that some whiskers are visible on the coatings after oxidation, which may result from slight oxidation of SiC and ZrC. In addition to the individual carbon fibers in the large pores, the fiber bundles inside the oxidized samples SZ19 and SZ20 are also well protected against oxidation and remain almost intact since they are completely enclosed by a dense ceramic coating (Fig. 12d and f). Unlike the individual carbon fibers inside the oxidized sample SZ20, the individual carbon fibers inside the oxidized sample S20 are burned-out completely after 5 h of oxidation, leaving behind many inter-connected hollow shells with

large pores (Fig. 12g). This means that oxygen has diffused to the surface of the PyC-coated carbon fibers through the pores in the SiC coating and reacts quickly with carbon before the continuous and dense ceramic coating can be formed. Regarding the fiber bundles inside the oxidized sample S20, a large number of carbon fiber filaments in the bundles are found to be severely oxidized and exhibit a typical needle-shaped morphology as shown in Fig. 12h, which would be expected to result in the degradation of the composite's properties.

4. Conclusions

SiC–ZrC ceramic coating on C/C composites was successfully prepared by reactive melt infiltration using a powdered mixture of Zr, Si and C as the infiltrator. The phase composition, microstructure and oxidation resistance of the resulting SiC–ZrC coated C/C composites are remarkably influenced by the infiltration temperature. When the RMI process is carried out at 1800 °C, a very thin coating mainly composed of SiC with some ZrC is formed on the surface of the C/C substrate. Only a small amount of molten Si infiltrates into the C/C substrate and reacts with carbon to form SiC whilst the Zr remains solid and thus immobile. With the increase of infiltration temperature from 1800 °C to 2000 °C, the average thickness of the ceramic coating formed on the C/C substrate increases significantly and the coating mainly consists of SiC, ZrC and a little ZrSi₂. Meanwhile, a large amount of SiC and ZrC are also formed in the pores within the C/C substrate and, as a result, the compactness of the C/C composites increases markedly. Sample SZ20 exhibits an excellent oxidation resistance. It gains weight about 5.9 wt% and its inner fiber bundles remain almost unaffected by oxygen attack after oxidation at 1550 °C in air for 5 h. However, under the same conditions, sample SZ18 loses 3.2 wt% of its initial weight because of the oxidation of part of the carbon fiber

filaments inside the fiber bundles. Compared with sample SZ20, the sample S20 shows a very poor oxidation resistance. It loses 44.3 wt% of its initial weight after exposure to static air at 1550 °C for 5 h. The outstanding oxidation resistance at 1550 °C in air for sample SZ20 can be mainly attributed to the rapid formation of a continuous and dense glass-like layer composed of ZrO_2 , $ZrSiO_4$ and SiO_2 on the surface of the composite during the oxidation, which effectively retards oxygen diffusion and consequent oxidation of the C/C substrate. On the other hand, the poor oxidation resistance at 1550 °C in air for sample S20 is mainly due to the fact that a continuous and dense SiO_2 layer cannot form rapidly on its surface by oxidation of its large SiC particles, leaving the sample surface open to rapid oxygen diffusion and consequent oxidation of the C/C substrate.

Acknowledgement

The authors acknowledge the financial support of the Key Program of Major Research Plan of the National Natural Science Foundation of China (Grant No. 91016003), and the Special Fund of the National Natural Science Foundation of China (Grant No. 51352001).

References

- [1] T. Windhorst, G. Blount, Carbon-carbon composites: a summary of recent developments and applications, *Mater. Des.* 18 (1997) 11-15.
- [2] J. Xie, K.Z. Li, H.J. Li, Q.G. Fu, L.J. Guo, Ablation behavior and mechanism of C/C–ZrC–SiC composites under an oxyacetylene torch at 3000 °C, *Ceram. Int.* 39 (2013) 4171-4178.
- [3] X. Yang, Q.Z. Huang, Z.A. Su, X. Chang, L.Y. Chai, C.X. Liu, L. Xue, D. Huang,

- Resistance to oxidation and ablation of SiC coating on graphite prepared by chemical vapor reaction, *Corros. Sci.* 75 (2013) 16-27.
- [4] H.J. Li, Q.G. Fu, X.H. Shi, K.Z. Li, Z.B. Hu, SiC whisker-toughened SiC oxidation protective coating for carbon/carbon composites, *Carbon* 44 (2006) 602-605.
- [5] L.F. Cheng, Y.D. Xu, L.T. Zhang, X.W. Yin, Preparation of an oxidation protection coating for C/C composites by low pressure chemical vapor deposition, *Carbon* 38 (2000) 1493-1498.
- [6] Y.L. Zhang, H.J. Li, Q.G. Fu, K.Z. Li, J. Wei, P.Y. Wang, A C/SiC gradient oxidation protective coating for carbon/carbon composites, *Surf. Coat. Technol.* 201 (2006) 3491-3495.
- [7] S.F. Tang, J.Y. Deng, W.C. Liu, K. Yang, Mechanical and ablation properties of 2D-carbon/carbon composites pre-infiltrated with a SiC filler, *Carbon* 44 (2006) 2877-2882.
- [8] Z. Wang, S.M. Dong, Y.S. Ding, X.Y. Zhang, H.J. Zhou, J.S. Yang, B. Lu, Mechanical properties and microstructures of C/SiC–ZrC composites using T700SC carbon fibers as reinforcements, *Ceram. Int.* 37 (2011) 695-700.
- [9] Y.L. Zhang, H.J. Li, X.F. Qiang, K.Z. Li, Oxidation protective C/SiC/Si-SiC multilayer coating for carbon/carbon composites applying at 1873 K, *J. Mater. Sci. Technol.* 26 (2010) 1139-1142.
- [10] S.F. Tang, J.Y. Deng, S.J. Wang, W.C. Liu, K. Yang, Ablation behaviors of ultrahigh temperature ceramic composites, *Mater. Sci. Eng. A* 465 (2007) 1-7.
- [11] Y.G. Wang, X.J. Zhu, L.T. Zhang, L.F. Cheng, C/C–SiC–ZrC composites fabricated by reactive melt infiltration with $\text{Si}_{0.87}\text{Zr}_{0.13}$ alloy, *Ceram. Int.* 38 (2012) 4337-4343.

- [12] L.H. Zou, N. Wali, J.M. Yang, N.P. Bansal, Microstructural development of a Cf/ZrC composite manufactured by reactive melt infiltration, *J. Eur. Ceram. Soc.* 30 (2010) 1527-1535.
- [13] Z.Q. Li, H.J. Li, S.Y. Zhang, K.Z. Li, Microstructure and ablation behaviors of integer felt reinforced C/C–SiC–ZrC composites prepared by a two-step method, *Ceram. Int.* 38 (2012) 3419-3425.
- [14] H.B. Li, L.T. Zhang, L.F. Cheng, Y.G. Wang, Ablation resistance of different coating structures for C/ZrB₂–SiC composites under oxyacetylene torch flame, *Ceram. Int.* 35 (2009) 2831-2836.
- [15] Q.M. Liu, L.T. Zhang, F.R. Jiang, J. Liu, L.F. Cheng, H. Li, Y.G. Wang, Laser ablation behaviors of SiC–ZrC coated carbon/carbon composites, *Surf. Coat. Technol.* 205 (2011) 4299-4303.
- [16] H.T. Wu, X. Wei, S.Q. Yu, W.G. Zhang, Ablation performances of multi-phased C/C–ZrC–SiC ultra-high temperature composites, *J. Inorg. Mater.* 26 (2011) 852-856.
- [17] Q.G. Li, S.M. Dong, P. He, H.J. Zhou, Z. Wang, J.S. Yang, B. Wu, J.B. Hu, Mechanical properties and microstructures of 2D Cf/ZrC–SiC composites using ZrC precursor and polycarbosilane, *Ceram. Int.* 38 (2012) 6041-6045.
- [18] H.B. Li, L.T. Zhang, L.F. Cheng, Y.G. Wang, Oxidation analysis of 2D C/ZrC–SiC composites with different coating structures in CH₄ combustion gas environment, *Ceram. Int.* 35 (2009) 2277-2282.
- [19] K.Z. Li, J. Xie, Q.G. Fu, H.J. Li, L.J. Guo, Effects of porous C/C density on the densification behavior and ablation property of C/C–ZrC–SiC composites, *Carbon* 57 (2013) 161-168.

- [20] Z.Q. Li, H.J. Li, S.Y. Zhang, J. Wang, W. Li, F.J. Sun, Effect of reaction melt infiltration temperature on the ablation properties of 2D C/C–SiC–ZrC composites, *Corros. Sci.* 58 (2012) 12-19.
- [21] Z.Q. Li, H.J. Li, S.Y. Zhang, W. Li, J. Wang, Microstructures and ablation properties of C/C–SiC–ZrC composites prepared using C/C skeletons with various densities, *Ceram. Int.* 39 (2013) 8173-8181.
- [22] Z.Q. Li, H.J. Li, W. Li, J. Wang, S.Y. Zhang, J. Guo, Preparation and ablation properties of ZrC–SiC coating for carbon/carbon composites by solid phase infiltration. *Appl. Surf. Sci.* 258 (2011) 565-571.
- [23] X. Yang, Z.A. Su, Q.Z. Huang, X. Fang, L.Y. Chai, Microstructure and mechanical properties of C/C–ZrC–SiC composites fabricated by reactive melt infiltration with Zr, Si mixed powders, *J. Mater. Sci. Technol.* 29 (2013) 702-710.
- [24] Y.G. Tong, S.X. Bai, K. Chen, C/C–ZrC composite prepared by chemical vapor infiltration combined with alloyed reactive melt infiltration, *Ceram. Int.* 38 (2012) 5723-5730.
- [25] S.A. Chen, C.R. Zhang, Y.D. Zhang, H.F. Hu, Influence of pyrocarbon amount in C/C preform on the microstructure and properties of C/ZrC composites prepared via reactive melt infiltration, *Mater. Des.* 58 (2014) 570-576.
- [26] Y.G. Wang, X.J. Zhu, L.T. Zhang, L.F. Cheng, Reaction kinetics and ablation properties of C/C–ZrC composites fabricated by reactive melt infiltration, *Ceram. Int.* 37 (2011) 1277-1283.
- [27] R.K. Rajput, *A Textbook of Manufacturing Technology: Manufacturing Processes*, Firewall Media, New Delhi, 2007.

- [28] X.Y. Yao, H.J. Li, Y.L. Zhang, H. Wu, X.F. Qiang, A SiC–Si–ZrB₂ multiphase oxidation protective ceramic coating for SiC-coated carbon/carbon composites, *Ceram. Int.* 38 (2012) 2095-2100.
- [29] T. Feng, H.J. Li, X.H. Shi, X. Yang, S.L. Wang, Oxidation and ablation resistance of ZrB₂-SiC-Si/B-modified SiC coating for carbon/carbon composites, *Corros. Sci.* 67 (2013) 292-297.
- [30] Z.J. Fan, Y.Z. Song, J.G. Li, L. Liu, J.R. Song, J.L. Chen, G.T. Zhai, J.L. Shi, Oxidation behavior of fine-grained SiC–B₄C/C composites up to 1400 °C, *Carbon* 41 (2003) 429-436.
- [31] Y.Q. Li, T. Qiu, Oxidation behaviour of boron carbide powder, *Mat. Sci. Eng. A-Struct.* 444 (2007): 184-191.

List of Figure captions

Fig. 1 (a) Low magnification SEM image of the porous C/C composites; (b) SEM image of the carbon fiber bundles with various orientations inside the C/C composites; (c) high magnification SEM image of a carbon fiber bundle inside the C/C composites; (d) magnification of some individual carbon fibers in Fig. 1(b).

Fig. 2 XRD patterns of the surface (a) and the cross section (b) of the samples prepared at various infiltration temperatures.

Fig. 3 Low magnification SEM images of the surface and the cross section of the samples prepared at various infiltration temperatures: (a, b) SZ18; (c, d) SZ19; (e, f) SZ20; (g, h) S20.

Fig. 4 Higher magnification SEM images of the surface and the cross section of the coatings on the samples prepared at various infiltration temperatures: (a, b) SZ18; (c, d) SZ19; (e, f) SZ20; (g, h) S20.

Fig. 5 EDS analysis of various locations shown in Fig. 4c and e.

Fig. 6 Linear EDS analysis in a cross section of the coating on sample SZ20.

Fig. 7 Surface morphology of the inner fibers in large voids in the composites prepared at various infiltration temperatures: (a) SZ18 (b) SZ19 (c) SZ20 (d) S20.

Fig. 8 Isothermal oxidation curves at 1550 °C in static air for samples SZ18, SZ19, SZ20 and S20.

Fig. 9 Surface and cross sectional morphologies of samples SZ18 (a, b), SZ19 (c, d), SZ20 (e, f) and S20 (g, h) after oxidation at 1550 °C for 5 h in static air.

Fig. 10 XRD patterns of the surface (a) and the cross section (b) of samples SZ18, SZ19,

SZ20 and S20 after oxidation at 1550 °C for 5 h in air.

Fig. 11 Linear EDS analysis in a cross section of sample SZ20 after oxidation at 1550 °C for 5 h in air.

Fig. 12 Morphologies of the inner single fibers and the fiber bundles inside samples SZ18 (a, b), SZ19 (c, d), SZ20 (e, f) and S20 (g, h) after oxidation at 1550 °C for 5 h in air.

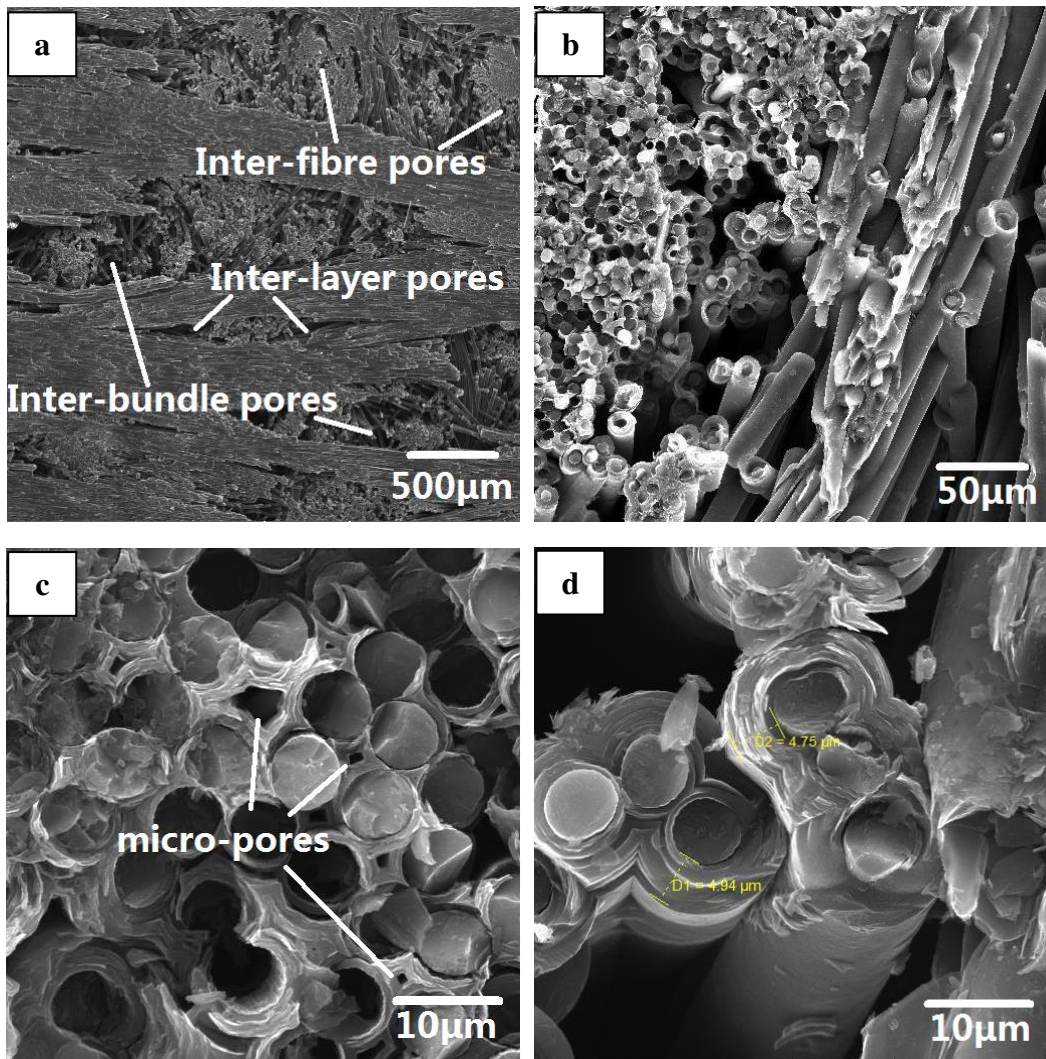


Fig. 1

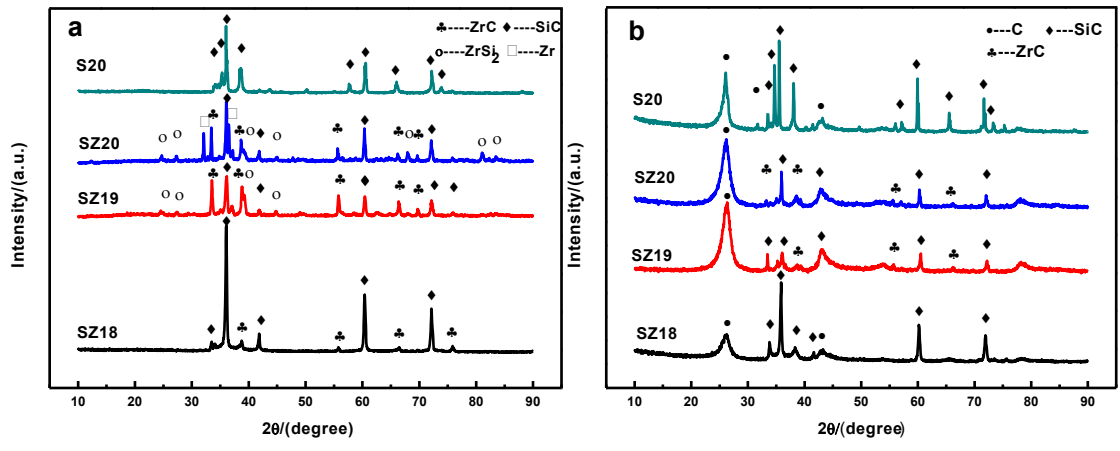


Fig. 2

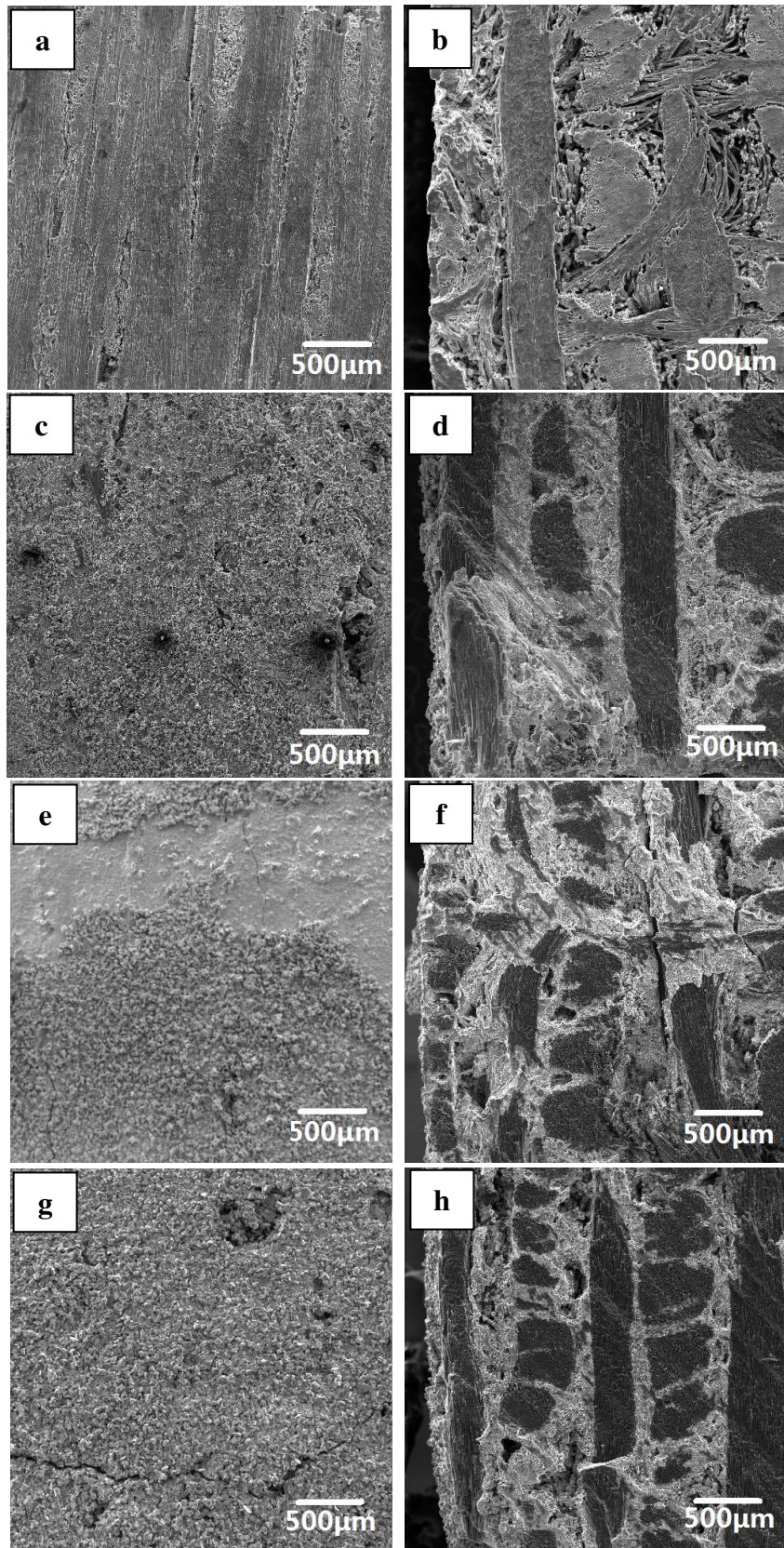


Fig. 3

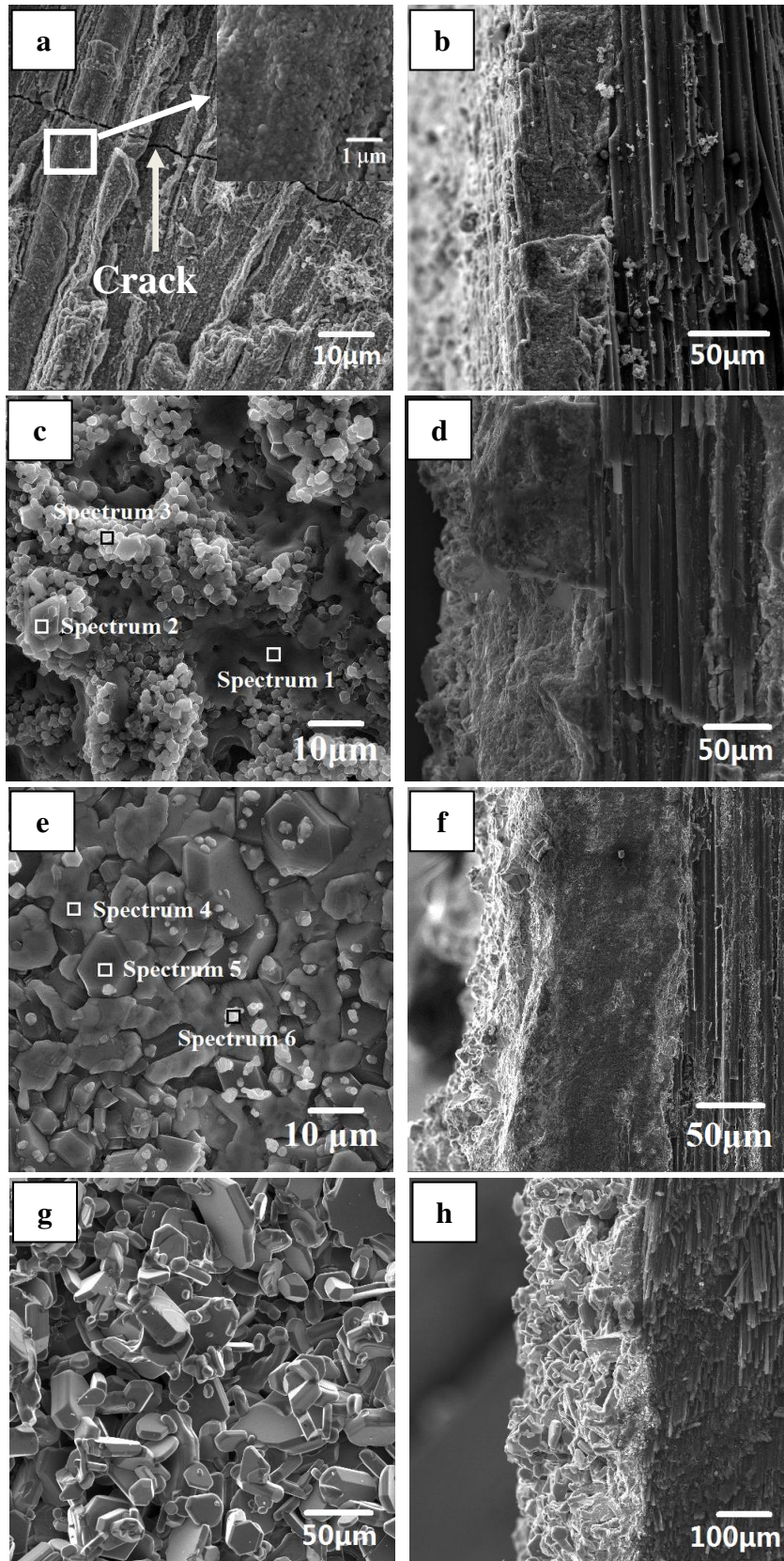


Fig. 4

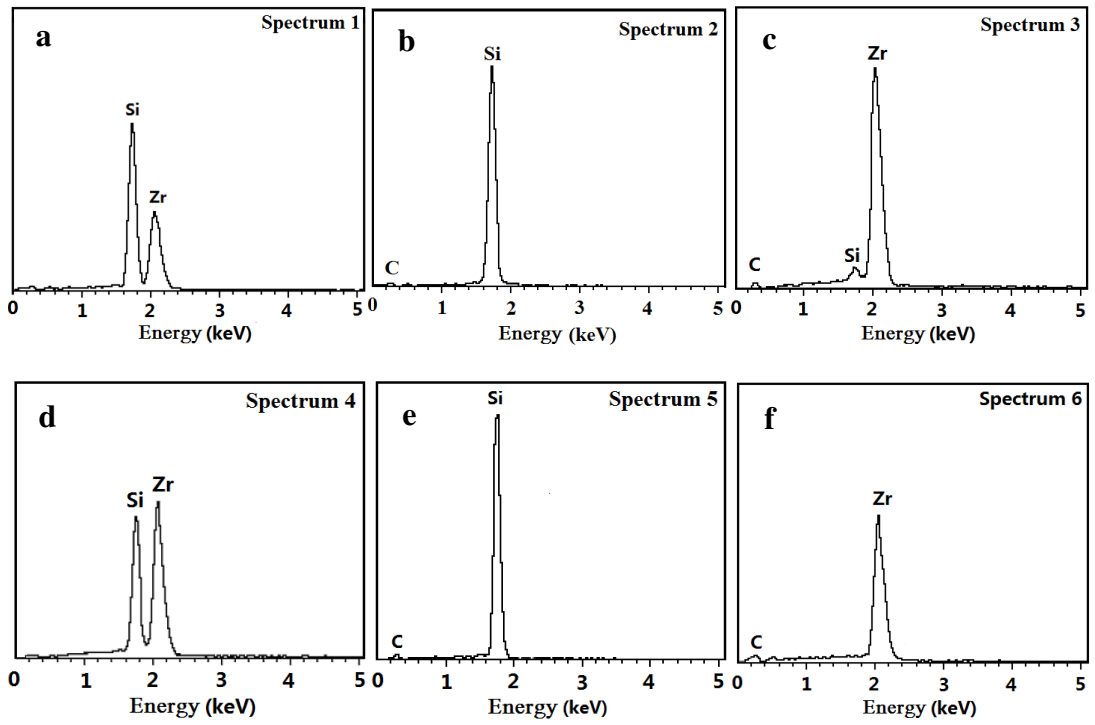


Fig. 5

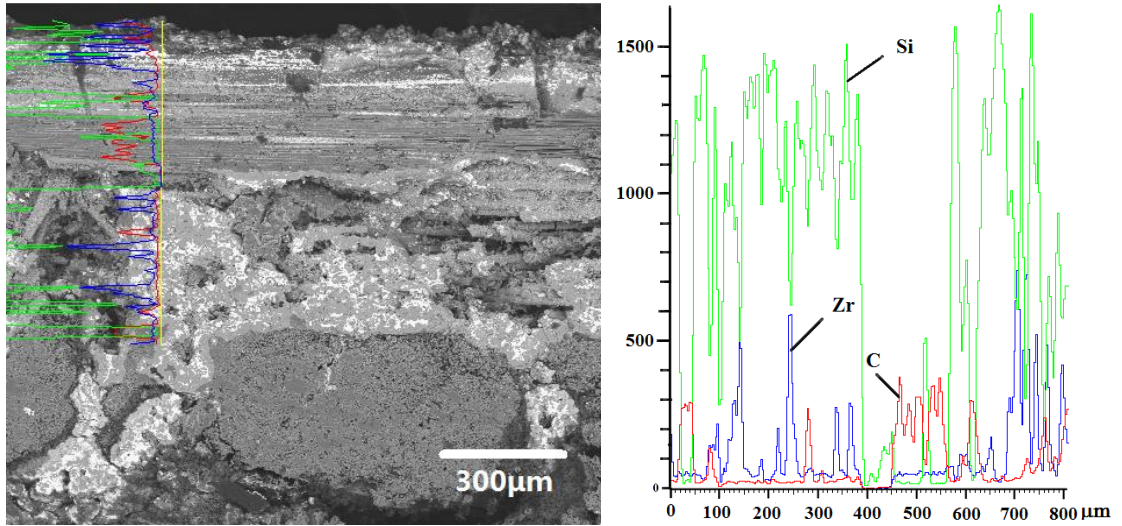


Fig. 6

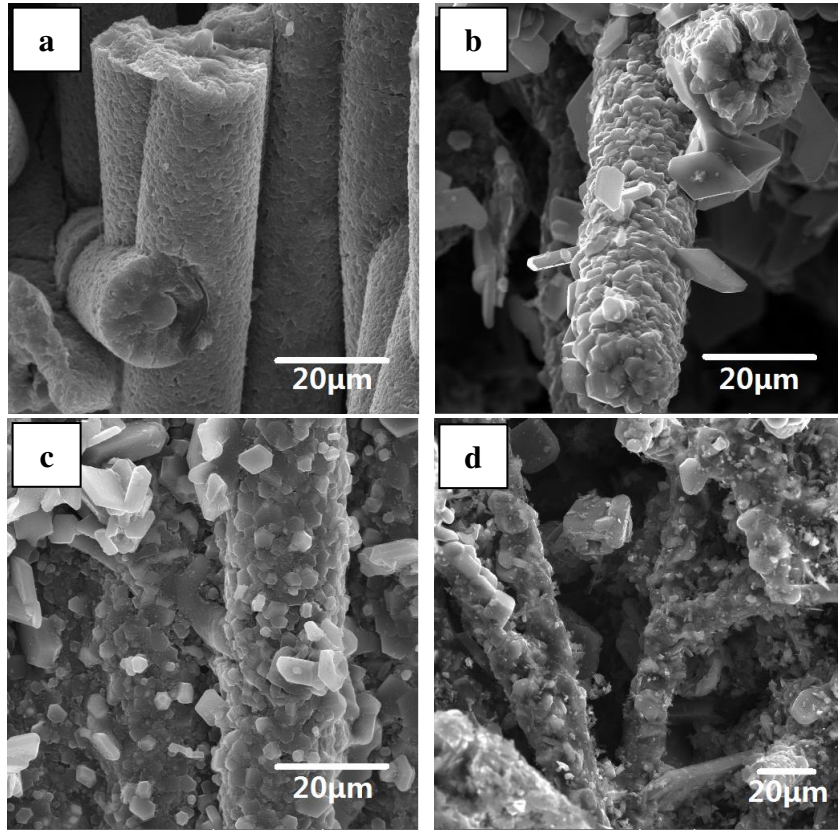


Fig. 7

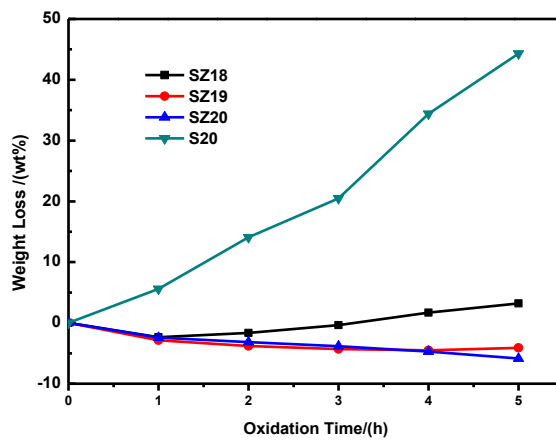


Fig. 8

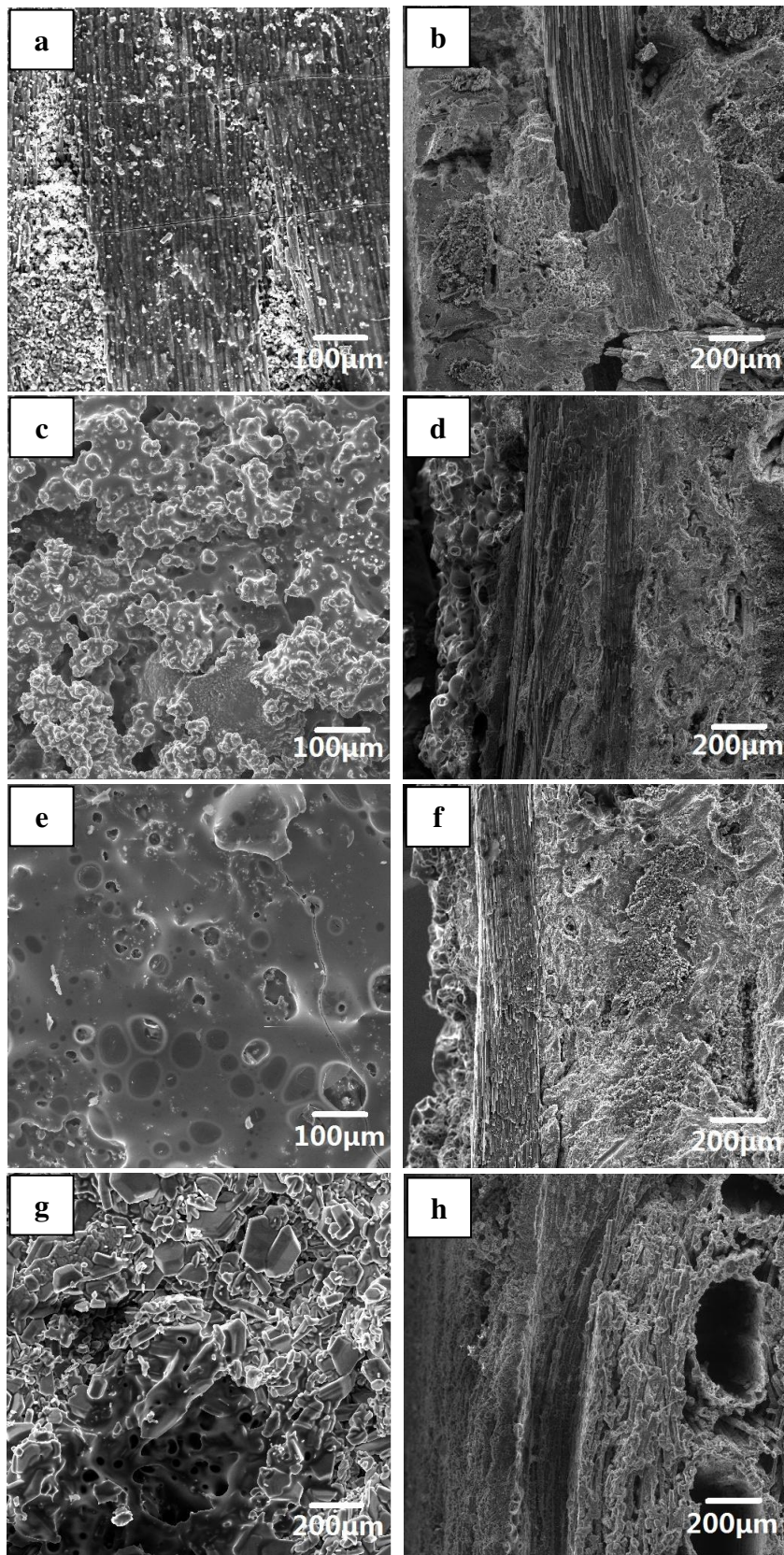


Fig. 9

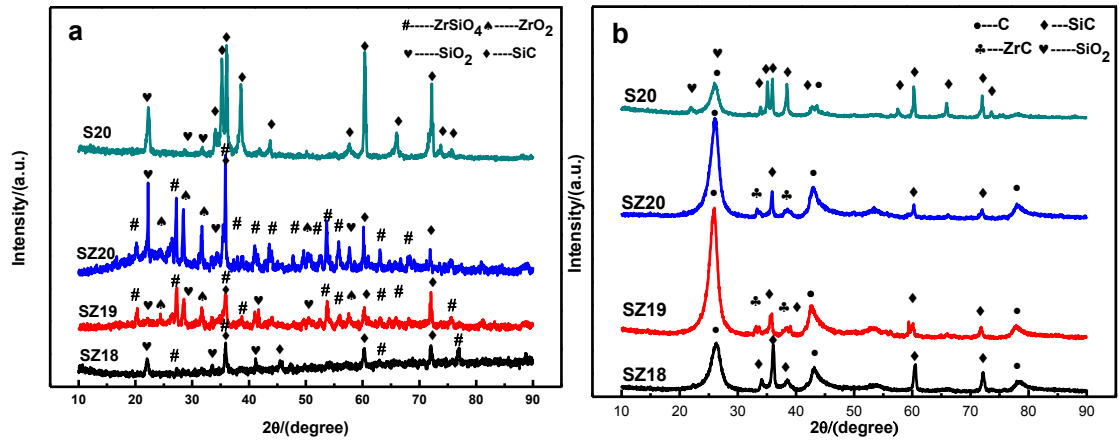


Fig. 10

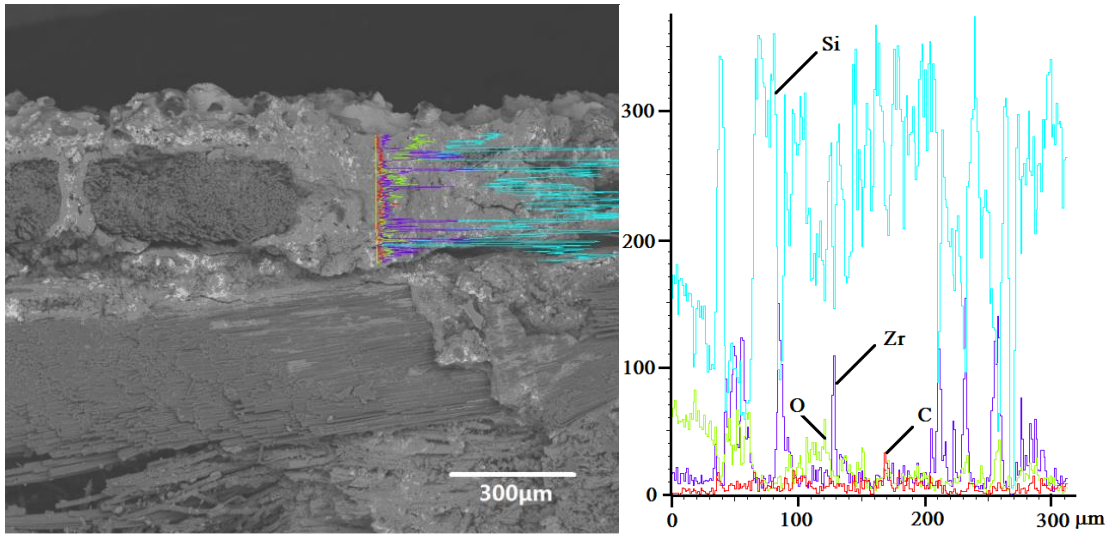


Fig. 11

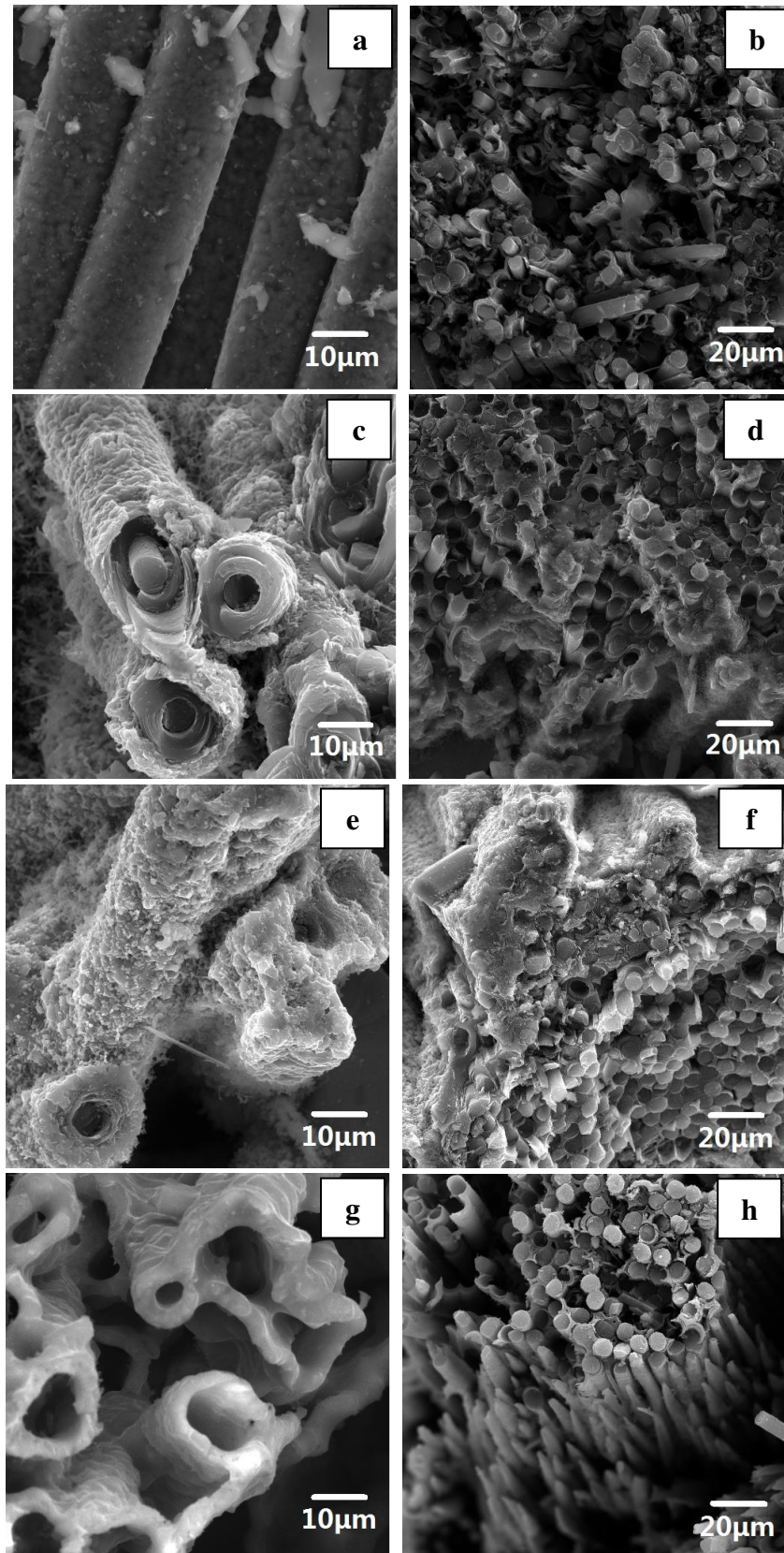


Fig. 12

